Published in final edited form as:
Atherosclerosis. 2019 January 1; 280: 28–36. doi:10.1016/j.atherosclerosis.2018.11.024.

MicroRNA-142-3p improves vascular relaxation in uremia

Máté Kétszeri[a], **Andrijana Kirsch**[b,c], **Bianca Frauscher**[a], **Foteini Moschovaki-Filippidou**[a], **Agnes A. Mooslechner**[a], **Alexander H. Kirsch**[a], **Corinna Schabhuettl**[a], **Ida Aringer**[a], **Katharina Artinger**[a], **Gudrun Pregartner**[d], **Robert Ekart**[e,f], **Silva Breznik**[g], **Radovan Hojs**[f,h], **Walter Goessler**[i], **Irene Schilcher**[b], **Helmut Müller**[j], **Barbara Obermayer-Pietsch**[k], **Saša Frank**[b], **Alexander R. Rosenkranz**[a], **Philipp Eller**[l,*], and **Kathrin Eller**[a]

[a]Department of Internal Medicine, Clinical Division of Nephrology, Medical University of Graz, Graz, Austria

[b]Gottfried Schatz Research Center for Cell Signaling, Metabolism and Aging, Molecular Biology and Biochemistry, Medical University Graz, Graz, Austria

[c]Department of Phoniatrics, ENT University Hospital Graz, Medical University of Graz, Austria

[d]Institute for Medical Informatics, Statistics and Documentation, Medical University of Graz, Graz, Austria

[e]Department of Dialysis, Clinic for Internal Medicine, University Clinical Centre Maribor, Slovenia

[f]Faculty of Medicine, University of Maribor, Maribor, Slovenia

[g]Department of Radiology, University Clinical Centre Maribor, Slovenia

[h]Department of Nephrology, Clinic for Internal Medicine, University Clinical Center Maribor, Slovenia

[i]Institute of Chemistry Analytical Chemistry, Karl-Franzens University Graz, Graz, Austria

[j]Department of Surgery, Division of Transplantation Surgery, Medical University of Graz, Graz, Austria

[k]Department of Internal Medicine, Division of Endocrinology and Diabetology, Medical University of Graz, Austria

[l]Department of Internal Medicine, Intensive Care Unit, Medical University of Graz, Austria

[*]Corresponding author. Clinical Intensive Care Unit, Department of Internal Medicine, Medical University of Graz, Auenbruggerplatz 15, A-8036 Graz, Austria. philipp.eller@medunigraz.at (P. Eller).

Conflicts of interest

The authors declared they do not have anything to disclose regarding conflict of interest with respect to this manuscript.

Author contributions

MK, AK, SF, KE and PE designed the experiments and interpreted the data. MK, BF, FM, AM, and CS performed and analysed the microbiological, histological and biochemical experiments; AK, IS, and SF performed and analysed the wire myography experiments; WG performed and analysed the mass spectrometry experiments; SB performed CT scans and analysed the calcium scores; RE and RH recruited and described the Slovenian cohort of ESRD patients; AHK, IA, KA, BO, HM, KE and ARR recruited and described the Austrian cohort of ESRD patients; GP performed the statistical analysis. MK, AK, SF, KE, and PE drafted the article. BF, FM, AM, AHK, CS, IA, KA, GP, RE, SB, RH, WG IS, BO, HM, SF, and ARR critically revised the article. All authors provided intellectual content of critical importance to the described work and approved the final version of the manuscript.

Europe PMC Funders Author Manuscripts

Abstract

Background and aims—Chronic kidney disease (CKD) is strongly associated with a high burden of cardiovascular morbidity and mortality. Therefore, we aimed to characterize the putative role of microRNAs (miR)s in uremic vascular remodelling and endothelial dysfunction.

Methods—We investigated the expression pattern of miRs in two independent end-stage renal disease (ESRD) cohorts and in the animal model of uremic DBA/2 mice *via* quantitative RT-PCR. Moreover, DBA/2 mice were treated with intravenous injections of synthetic miR-142-3p mimic and were analysed for functional and morphological vascular changes by mass spectrometry and wire myography.

Results—The expression pattern of miRs was regulated in ESRD patients and was reversible after kidney transplantation. Out of tested miRs, only blood miR-142-3p was negatively associated with carotid-femoral pulse-wave velocity in CKD 5D patients. We validated these findings in a murine uremic model and found similar suppression of miR-142-3p as well as decreased acetylcholine-mediated vascular relaxation of the aorta. Therefore, we designed experiments to restore bioavailability of aortic miR-142-3p *in vivo* via intravenous injection of synthetic miR-142-3p mimic. This intervention restored acetylcholine-mediated vascular relaxation.

Conclusions—Taken together, we provide compelling evidence, both in humans and in mice, that miR-142-3p constitutes a potential pharmacological agent to prevent endothelial dysfunction and increased arterial stiffness in ESRD.

Keywords

Arterial stiffness; Endothelium dysfunction; Pulse wave velocity; Vascular calcification

1 Introduction

Chronic kidney disease (CKD) significantly increases cardiovascular morbidity and overall mortality [1]. Patients suffering from end-stage renal disease (ESRD) have a ten-to hundred-fold increased risk for cardiovascular morbidity and mortality compared to patients with normal kidney function, which is not adequately predicted by traditional risk factors [2]. This massive burden of cardiovascular disease in CKD and ESRD is strongly associated with uremic media calcification, left ventricular hypertrophy, and sudden cardiac death [3,4]. These morphological cardiovascular changes are paralleled by a reduced vascular compliance and an impairment of endothelium-dependent and -independent vascular function in patients with CKD [5,6]. Cardiovascular disease in ESRD is largely not explained by traditional risk factors and does not respond to available pharmacological treatment options including statins [7–9]. It has been shown that uremic vascular disease is driven by multiple factors, including disturbances in mineral and bone metabolism, on the one hand, and uremic toxicity on the other hand [10,11].

In uremia, the vascular response to hemodynamic stress is orchestrated by a complex interplay of regulators that on a morphological level culminates in vascular calcification and functionally is due to transdifferentiation of vascular smooth muscle cells (VSMC) from contractile to proliferative, osteoblastic, and/or inflammatory phenotypes, on the one hand,

and endothelial dysfunction on the other hand. There is preliminary evidence that miRs play a central role in this VSMC phenotypic modulation and dysfunction of endothelial cells in uremia [11–15]. Therefore, we designed clinical and experimental studies to investigate the specific role of miRs in vascular adaptation during CKD, to explore the mechanisms on miR-mediated vascular dysfunction, and to test the feasibility of using miRs as pharmacological tools to prevent the deleterious cardiovascular complications in ESRD.

2 Materials and methods

2.1 Study population, pulse wave velocity and computed tomography

We prospectively enrolled 53 consecutive hemodialysis (HD) patients at the Department of Dialysis of the University Clinical Centre Maribor, Slovenia, and 9 consecutive peritoneal dialysis (PD) patients at the Clinical Division of Nephrology of the Medical University of Graz, Austria. The PD patients were recruited immediately prior to kidney transplantation and controlled after one year. The 8 Austrian healthy controls were matched for sex (63% male) and age (46.9 ± 3.6 years). All of them had no relevant medical history, and did not take any regular medication. The study protocols were approved by the respective Institutional Review Boards of the University Clinical Centre Maribor (UKC-MB-KME-90/14) and the Medical University of Graz (25–207/ex 12/13), and complied with the Declaration of Helsinki. After obtaining written informed consent from the patients, peripheral blood was collected in PAXgene Blood RNA tubes (Qiagen, Venlo, Netherlands).

Carotid-femoral pulse wave velocity (cfPWV) was performed in all HD patients in the morning between 8:00 and 11:00 under standardized conditions. Prior to the measurement, subjects were under similar conditions (abstained from coffee, cigarettes, heavy meals, and exercise). Each patient waited for 5–10 min in a quiet room before blood pressure recordings and cfPWV were taken. Before the cfPWV measurement office brachial diastolic and systolic blood pressure (BP) values have been obtained from the portable bedside monitoring automatic BP device (Dash 4000, General Electric Healthcare, Dallas, TX, USA). cfPWV was recorded using applanation tonometry (SphygmoCor, AtCor Medical, Ltd., Sydney, Australia). A single examiner performed all measurements. cfPWV was evaluated between the carotid and femoral artery with the participant lying in the supine position. Pulse measurements were performed non-invasively over the carotid and femoral artery while an ECG recording was performed simultaneously. A minimum of 12 s of signal (approximately 10 heart beats) was recorded after a strong accurate and reproducible pulse wave signal was obtained. The distance from the carotid to femoral artery was measured directly between each artery location and the supra-sternal notch and the values were entered into the SphygmoCor software database. cfPWV was calculated by measuring the time delay between two characteristic timing points on two pressure waveforms that were at a known distance apart. The SphygmoCor method uses the foot of the waveform as an onset point for calculating the time differences between the R wave of the ECG and the pulse waveforms at each site. cfPWV was automatically calculated by the Atcor software as the carotid-femoral artery distance divided by the wave travelling time between the above 2 measuring sites. In each patient, a minimum three cfPWV measurements were performed. The measurements

with a standard deviation less than 10% and the average of these measurements were used for analysis.

After cfPWW measurement ambulatory blood pressure monitoring was done for 48-h using a Schiller BR-102 plus monitor (Schiller, Dietikon, Switzerland). Blood pressure was recorded every 20 min during the day and every 30 min during the night. The cuff of the blood pressure monitor was applied to the upper portion of the arm, and the patients were instructed to attend to their usual activities and medications.

The computed tomography (CT) examinations of heart and pelvis were routinely performed on a Toshiba Aquilion 64-row detector CT scanner (Toshiba Medical Systems, Minato, Japan). The calcium score for coronary arteries, ascending thoracic, and infrarenal abdominal aorta was calculated by multiplying the calcification areas in mm^2 by a density score determined from the peak CT scan number (Agatston score) with a dedicated software (TeraRecon, Foster City, CA, USA) as previously described [16].

2.2 Design of animal experiments

Female eight to ten week old dilute-brown agouti 2 (DBA/2NCrl, hereafter referred to as DBA/2) mice were obtained from Charles River (Sulzfeld, Germany) and housed in a virus/antibody-free environment. These mice have an inherent susceptibility to high-phosphate diet-triggered calcification [17–19]. To induce media calcification, they were placed on high-phosphate diet (HPD) from Altromin (Lage, Germany) containing 20.2 g phosphorus, 9.4 g calcium, 0.7 g magnesium, and 500 IU vitamin D3 per kg. The standard chow contained 7.0 g phosphorus, 10.0 g calcium, 2.2 g magnesium, and 1000 IU vitamin D3 per kg. Mice were then followed for 11 days and culled under anaesthesia. Female eight to ten weeks old C57BL/6J mice from Charles River were used in the same setup. All animal experiments were approved by Austrian veterinary authorities (BMWF-66.010/0061-WF/V/3b/2016) and corresponded to directive 2010/63/EU of the European Parliament. In a second set of experiments, female DBA/2 mice were again fed HPD for 11 days and then sacrificed under anaesthesia. On day 9, the mice were injected with the syn-mmu-mir-142-3p miR mimic (Qiagen, Venlo, Netherlands) or negative control siRNA (Qiagen) via the tail vein using the in vivo-JetPEI transfection reagent (Polypus transfection SA, Illkirch-Graffenstaden, France). Each mouse received 2 nmol syn-mmu-mir-142-3p miR mimic or 2 nmol Allstars Negative Control siRNA (Qiagen) as control with 4.28 μl in vivo-JetPEI transfection reagent in a final volume of 200 μl.

2.3 miR isolation, reverse transcription quantitative PCR

From mice, 100 μl peripheral blood was collected in RNAprotect Animal Blood Tubes (Qiagen), after which the tubes were incubated at room temperature for 3 h and stored at −80 °C. Total RNA was isolated using the RNeasy Protect Animal Blood Kit (Qiagen), strictly following the manufacturer's instructions. Aortas from mice were stored in RNAlater (Sigma-Aldrich, St. Louis, MO, USA) at −80 °C and the *mir*Vana miRNA Isolation Kit (Thermo Fisher Scientific, Waltham, MA, USA) was used to isolate RNA. From humans, total RNA was isolated using the PAXgene Blood miRNA kit (Qiagen), strictly following the manufacturer's instructions. 200 ng total RNA was reverse transcribed with the miScript

II RT Kit (Qiagen) using the miScript HiFlex Buffer. Real time quantitative PCR (RT-qPCR) was carried out on a CFX96 Real-Time PCR Detection System (Biorad, Hercules, CA, USA) using the miScript SYBR Green PCR kit (Qiagen) with the following miScript Primer Assays (Qiagen): Hs_miR-21_2 (MS00009079), Hs_miR-21*_1 (MS00009086), Hs_miR-26b_1 (MS00003234), Hs_miR-98_1 (MS00003367), Hs_miR-98-3p_1 (MS00045136), Hs_miR-103a_1 (MS00031241), Hs_miR-125b_1 (MS00006629), Hs_miR-142-3p_2 (MS00031451), Hs_miR-145_1 (MS00003528), Hs_miR-146a_1 (MS00003535), Hs_miR-146a*_1 (MS00008715), Hs_miR-155_2 (MS00031486), Hs_miR-155*_1 (MS00008778), Hs_miR-191_1 (MS00003682), Hs_miR-210_1 (MS00003801), Hs_miR-210-5p_1 (MS00045836), Hs_miR-223_1 (MS00003871), Hs_miR-223*_1 (MS00009184), Hs_miR-423-5p_1 (MS00009681), Hs_RNU6-2_11 (MS00033740). 2 ng reverse transcription product was used for each RT-qPCR reaction. RT-qPCR was evaluated using the ΔΔCq method. The miR expressions were normalized to the endogenous housekeeper RNU6b small nuclear RNA.

2.4 Biochemical analyses

BUN levels were measured using the SPOTCHEM EZ SP-4430 automated analyser (Arkray, Kyoto, Japan) with the appropriate test tubes and test strips (Menarini diagnostics, Vienna, Austria). Renal calcium content was determined using the Calcium Detection Assay Kit from Abcam (Cambridge, United Kingdom) following the manufacturer's instructions and normalized to the tissue weight.

2.5 Histology

Histological evaluations were performed as previously described [18]. The slides were evaluated, and pictures were taken with an Olympus BX43 light microscope and the cellSens Entry 1.14 program (Olympus, Shinjuku, Tokyo, Japan). PAS positive tubular casts were counted in 18 high power fields on 3 kidney sections per sample by two blinded and independent evaluators.

2.6 Mass spectrometry

Aortas were isolated from the mice, stored at −80 °C and freeze-dried as previously described [18]. The concentrations of Ca, Mg and P were determined with an inductively coupled plasma mass spectrometer (Agilent 7700x, Agilent, Waldbronn Germany), and Be and Ge were added online as internal standards during the measurement.

2.7 Wire myography

Wire myography was done as previously described [20]. Briefly, mouse aortic rings 2 mm in length were isolated and positioned in small wire myograph chambers (Danish MyoTechnology, Aarhus, Denmark) containing physiological salt solution (PSS) (114 mM NaCl, 4.7 mM KCl, 0.8 mM KH_2PO_4, 1.2 mM $MgCl_2$, 2.5 mM $CaCl_2$, 25 mM $NaHCO_3$ and 11 mM D-glucose pH 7.4). PSS containing 60 mM KCl (KPSS) was used to determine maximum contractility of the vessels. The rings were precontracted with increasing concentrations of norepinephrine (NE) (1nM-1μM), followed by endothelium-dependent relaxation to cumulatively increasing concentrations of acetylcholine chloride (ACh)

(1nM-10μM). The endothelium-independent relaxation was examined by exposure of rings to increasing concentrations of sodium nitroprusside (SNP) (1nM-1μM), a nitric oxide (NO) donor. Relaxation values were expressed as a percentage of the initial NE-induced contraction. To examine the involvement of prostanoids, 10 μM diclofenac was added to the PSS during the myography procedure. The NO bioavailability was estimated from the constriction response to eNOS inhibitor Nω-nitro-L-arginine (L-NNA, 300 μM) in aortic rings precontracted with norepinephrine to 10% of the maximal contraction in the presence of diclofenac (10 μM).

2.8 Thromboxane release from aortic rings ex vivo

Aortic rings were placed in separate wells of a 96-well plate in 150 μl DMEM (Sigma-Aldrich) supplemented with 10% FCS (Sigma-Aldrich) for 1 h under cell culture conditions (37 °C, 5% CO_2). The rings were then washed and stimulated with 10 μM ACh in DMEM without FCS for 10 min. After the stimulation the supernatants were collected and Thromboxane B_2 (TXB_2) was measured by a Thromboxane B_2 Parameter Assay Kit (R&D Systems, Minneapolis, MN, USA), following the manufacturers' instructions.

2.9 Statistical analysis

Data are presented as mean ± SEM or as median (25th, 75th percentile). Normal distribution of the data was assessed by the Kolmogorov-Smirnov test with Lilliefors correction. Linear regression analyses were performed to assess the association between blood miR levels and functional and morphological cardiovascular parameters, such as the carotid-femoral pulse wave velocity and calcium scores of the coronary arteries as well as the thoracic and abdominal aorta within the Slovenian cohort of CKD 5D patients. In addition to univariable analyses, we also adjusted for age, dialysis vintage, and insulin therapy, which are known confounders of vascular calcification and arterial stiffness. Differences between DBA/2 treatment groups were compared by either the non-parametric Mann-Whitney *U* test or the unpaired Student's t-test as appropriate depending on the distribution of the tested variable. The significance level was set to 5%. The statistical analyses were performed using GraphPad Prism 7.0 (GraphPad, La Jolla, CA) and R version 3.3.3.

3 Results

3.1 miR-142-3p is associated with pulse-wave velocity in ESRD patients

We investigated the expression pattern of 19 blood miRs that might play a role in vascular remodelling and/or endothelial dysfunction in patients with chronic kidney disease (CKD) stage 5 on dialysis and found a conserved miR expression pattern in two independent cohorts (Fig. 1). The clinical and biochemical characteristics of these patients are given in Table 1. Interestingly, this miR profile was independent of the type of dialysis (hemodialysis *vs.* peritoneal dialysis), age and dialysis vintage, and was reversible after kidney transplantation, as shown by the subgroup of Austrian patients who were followed-up one year after kidney transplantation (Table 1 and Supplementary Table 1), indicating that it might be an early event in the pathological reaction to uremia. Next, we used linear regression analyses to assess the association between these blood miR levels and functional as well as morphological cardiovascular parameters in the Slovenian cohort of 53 CKD 5D

patients. For this purpose, we used pulse wave velocity and calcium score as dependent variables. Among the investigated miRs, only miR-142-3p displayed a significant negative association with the carotid-femoral pulse wave velocity ($p = 0.025$) (Supplementary Table 2). However, there was no significant association of blood miR-142-3p ($p = 0.91$) or other tested miRs with calcium scores of the coronary arteries, thoracic or abdominal aorta. When adjusting the univariable models for age, dialysis vintage, and insulin therapy, there was still a trend for an association of miR-142-3p with carotid-femoral pulse wave velocity ($p = 0.062$).

In order to validate these findings of our observational bi-centric pilot study, we investigated the miR expression pattern in a murine CKD model and respective murine controls. For this purpose, we used DBA/2 and C57BL/6 mice that were exposed to high-phosphate diet as previously described [17–19]. Due to their distinct genetic background, DBA/2 mice develop a phosphate-induced nephropathy, whereas C57BL/6 do not show any renal phenotype. As shown in Supplementary Table 1, there were similar miR regulation patterns both in the blood of uremic mice and ESRD patients. Moreover, miR regulation was not directly induced by the high-phosphate diet, as C57BL/6 mice on high-phosphate diet had no renal disease and showed the same expression pattern as C57BL/6 mice on standard chow, whereas DBA/2 mice on high-phosphate diet had overt phosphate-induced nephropathy and a similar miR expression profile as patients with CKD stage 5 on dialysis. These miR expression patterns were seen both in blood samples and in aortic tissue of DBA/2 mice.

3.2 Intravenous injection of syn-mmu-mir-142-3p restores miR-142-3p bioavailability

As only miR-142-3p displayed a significant negative association with the carotid-femoral pulse wave velocity, we specifically focused on this miR. As shown in Fig. 2A, miR-142-3p blood levels were significantly lower in dialysis patients and returned to levels of healthy controls after kidney transplantation. A similar downregulation occurred in DBA/2 mice fed with high-phosphate diet and was not observed in C57BL/6 mice on high-phosphate diet. In order to investigate the functional implications of this downregulation, we restored the bioavailability of miR-142-3p by intravenous injection of synthetic mimic syn-mmu-mir-142-3p. With this experimental intervention, we successfully restored aortic miRNA-142-3p bioavailability *in vivo* in our animal model (Fig. 2B). Importantly, mice treated with syn-mmu-mir-142-3p showed a similar amount of renal calcification (Fig. 3A–C,H) and PAS positive tubular casts (Fig. 3D–F,I) with similarly elevated blood urea nitrogen (Fig. 3G) compared to negative control siRNA treated controls. On the other hand, C57Bl/6 mice on high-phosphate diet displayed normal renal function and did not show any regulation of miR-142-3p expression both in blood and in aorta when exposed to high-phosphate diet (Supplementary Fig. 1, Supplementary Table 1), thus excluding a direct specific effect of the high-phosphate diet on the miR-142-3p regulation.

3.3 Syn-mmu-mir-142-3p improves aortic relaxation attenuated by uremia

To dissect the specific impact of miR-142-3p on vascular phenotype and function, we designed mass spectrometry experiments of explanted murine aortas and ex vivo bioassay experiments with aortic rings. In mass spectrometry, there was no discernible effect of syn-mmu-mir-142-3p injection on the amount of vascular calcification in aortas of uremic

DBA/2 mice (Supplementary Table 3). In wire myography, uremia significantly increased the maximum KPSS-mediated contraction of aortic rings, while there was no effect on norepinephrine (NE)-mediated contraction. These phenomena were not affected by synthetic miR treatment (Fig. 4A and B). Uremia caused a marked impairment of acetylcholine (ACh)-induced relaxation of NE-precontracted aortic rings, when compared to non-uremic animals (Fig. 4C). Importantly, when mice were injected with syn-mmu-mir-142-3p 2 days before sacrifice, ACh-induced relaxation of aortic rings from uremic DBA/2 mice was restored to control levels (Fig. 4C). Neither kidney disease nor reversal of miR-142-3p down-regulation had any effect on sodium nitroprusside (SNP)-mediated relaxation (Fig. 4D). To identify mechanisms responsible for syn-mmu-mir-142-3p-mediated restoration of ACh-induced relaxation of rings from uremic mice, we first examined the role of endothelial-derived constricting prostanoids and found a significant down-regulation of the potent vasoconstrictor thromboxane B_2 (TXB_2) in the supernatant of aortic rings, when comparing syn-mmu-mir-142-3p treated mice to respective negative controls (0.25 ± 0.02 ng/ml *vs.* 0.46 ± 0.03 ng/ml; n = 8 *vs.* n = 6; $p < 0.0001$) (Fig. 4E). Therefore, myography was done in the presence of a cyclooxygenase inhibitor, diclofenac. As shown in Fig. 4F, diclofenac had no effect on the HPD-induced impairment of ACh-induced relaxation and did not abolish the effect of syn-mmu-mir-142-3p on ACh-induced relaxation. These findings suggested that the contribution of syn-mmu-mir-142-3p –mediated changes of prostanoid synthesis plays a minor role in the recovery of relaxation and that additional mechanisms are involved. We next analysed the impact of our intervention on the basal NO bioavailability, and determined the L-NNA-induced endothelium-dependent constrictor response in NE-preconstricted aortic rings. This constrictor response, indicative of basal NO bioavailability, was markedly decreased in aortic rings of uremic mice compared to healthy mice, and was not restored after syn-mmu-mir-142-3p injection (Fig. 4G). From these results we concluded that uremia decreases the basal NO bioavailability and ACh-induced relaxation, whereby the latter can be recovered by syn-mmu-mir-142-3p treatment.

4 Discussion

The endothelium regulates vascular tone via endothelium-derived factors that maintain a balance between vasoconstriction and vasodilatation [21]. We here provide evidence for miRNA involvement in uremic endothelial dysfunction and show that blood miR-142-3p levels are not only associated with parameters of vascular relaxation both in ESRD patients and uremic mice, but rather play a pathogenic role, since counteracting miR-142-3p downregulation restored ACh-mediated vascular relaxation. To our knowledge, this is the first study to provide direct functional evidence of an *in vivo* effect of miRNAs in uremic vascular disease. Thus, we extend previous findings by Zhang et al., who found that miR-142 promotes the expression of eNOS in human peripheral blood-derived endothelial progenitor cells *in vitro* [22]. Moreover, these findings are in line with Sharma et al., who demonstrated that miR-142 is a critical element of adaptive cardiac hypertrophy in response to hemodynamic stress [12]. In our hands, blood miR-142-3p is not just a mere biomarker of impaired renal function and endothelial dysfunction, but represents a direct mediator of impaired ACh-mediated vascular relaxation in uremia and in this manner constitutes a potential pharmacological target to prevent the deleterious arterial stiffness in uremia.

In uremia there are profound vascular disturbances that affect both VSMC and endothelial cells and are associated with a high cardiovascular morbidity and mortality. While there is evidence that miRs do affect the development of uremic media sclerosis, the evidence on miR involvement in functional impairment of vessels in uremia is only beginning to emerge. Thus, our data are also in line with Shang et al. who showed uremic serum to induce miR-92 expression in cultured endothelial cells and found this miR-92 to be associated with levels of uremic toxins in CKD patients [23].

The exact mode of action of miR-142-3p to improve ACh-mediated vascular relaxation was not merely attributable to an attenuation of constricting prostanoids and not associated with a change in basal NO bioavailability, as shown by the L-NNA-induced endothelium-dependent constrictor response in NE-preconstricted aortic rings. However, our experiments of basal NO bioavailability in explanted aortic rings do not exclude in a strict sense an augmented NO bioavailability after endothelial activation *in vivo*. Possible mechanisms underlying recovery of ACh-induced relaxation in uremic mice by syn-mmu-mir-142-3p treatment might include increased induction of the eNOS activating pathway due to increased efficacy of ACh-induced signalling, augmented activating (Ser-1177) or attenuated inhibitory (Tyr 495) phosphorylation, or altered eNOS intracellular localization. The potential therapeutic application of miR-142-3p might be limited by the fact that miR-142 also controls mature T cell responses and hematopoietic lineage formation [24–27]. These potential additional effects deserve further evaluation, especially when considering long-term therapeutic treatments with synthetic miR-142-3p mimics. Moreover, the small sample size of the healthy control population and of ESRD patients who were also controlled one year after kidney transplantation constitutes a major limitation of this study.

In the present setup, our experimental intervention with intravenous injection of syn-mmu-mir-142-3p had no effect on the absolute amount of vascular calcification, which nicely reflects the results in humans, where there was a negative association of mir-142-3p blood levels with carotid-femoral pulse wave velocity but no association with the degree of vascular calcification as assessed by computed tomography. This discrepancy between functional and morphological changes in uremic vessels stresses the notion that endothelial dysfunction with impaired ACh-mediated vascular relaxation significantly contributes to arterial stiffness and may precede morphological changes in the tunica media with VSMC phenotypic transdifferentiation. Indeed, the regulation of miR profile was reversible after kidney transplantation and was independent of dialysis modality, age and dialysis vintage.

Taken together, pharmacological exploitation of naturally occurring miRs and especially miR-142-3p could be a potential avenue to counteract vascular dysfunction in uremia and might thus ultimately prevent deleterious cardiovascular endpoints in patients with ESRD.

Supplementary Material

Refer to Web version on PubMed Central for supplementary material.

Acknowledgements

We thank Margarete Lechleitner for her excellent technical work.

Financial support

This work was supported by the Austrian Science Funds (FWF) to PE and KE (P27537-B26) and to SF (P27166-B23). MK and BF are enrolled in the PhD program in molecular medicine; AAM and FM are enrolled in the PhD program MOLIN at the Medical University of Graz.

References

[1]. Go AS, Chertow GM, Fan D, McCulloch CE, Hsu CY. Chronic kidney disease and the risks of death, cardiovascular events, and hospitalization. N Engl J Med. 2004; 351:1296–1305. [PubMed: 15385656]

[2]. Sarnak MJ, Levey AS, Schoolwerth AC, et al. Kidney disease as a risk factor for development of cardiovascular disease: a statement from the American heart association councils on kidney in cardiovascular disease, high blood pressure research, clinical cardiology, and epidemiology and prevention. Circulation. 2003; 108:54–69. [PubMed: 12821550]

[3]. Witteman JC, Kok FJ, van Saase JL, Valkenburg HA. Aortic calcification as a predictor of cardiovascular mortality. Lancet. 1986; 2:1120–1122. [PubMed: 2877272]

[4]. Wilson PW, Kauppila LI, O'Donnell CJ, et al. Abdominal aortic calcific deposits are an important predictor of vascular morbidity and mortality. Circulation. 2001; 103:1529–1534. [PubMed: 11257080]

[5]. Blacher J, Guerin AP, Pannier B, Marchais SJ, London GM. Arterial calcifications, arterial stiffness, and cardiovascular risk in end-stage renal disease. Hypertension. 2001; 38:938–942. [PubMed: 11641313]

[6]. Kopel T, Kaufman JS, Hamburg N, Sampalis JS, Vita JA, Dember LM. Endothelium-dependent and –independent vascular function in advanced chronic kidney disease. Clin J Am Soc Nephrol. 2017; 12:1588–1594. [PubMed: 28784655]

[7]. Karumanchi SA, Thadhani R. Kidney complications: why don't statins always work? Nat Med. 2010; 16:38–40. [PubMed: 20057425]

[8]. Wanner C, Krane V, März W, et al. Atorvastatin in patients with type 2 diabetes mellitus undergoing hemodialysis. N Engl J Med. 2005; 353:238–248. [PubMed: 16034009]

[9]. Fellström BC, Jardine AG, Schmieder RE, et al. Rosuvastatin and cardiovascular events in patients undergoing hemodialysis. N Engl J Med. 2009; 360:1395–1407. [PubMed: 19332456]

[10]. Jourde-Chiche N, Dou L, Cerini C, Dignat-George F, Brunet P. Vascular incompetence in dialysis patients–protein-bound uremic toxins and endothelial dysfunction. Semin Dial. 2011; 24:327–337. [PubMed: 21682773]

[11]. Paloian NP, Giachelli C. A current understanding of vascular calcification in CKD. Am J Physiol Renal Physiol. 2014; 307:F891–F900. [PubMed: 25143458]

[12]. Sharma S, Liu J, Wei J, Yuan H, Zhang T, Bishopric NH. Repression of miR-142 by p300 and MAPK is required for survival signalling via gp130 during adaptive hypertrophy. EMBO Mol Med. 2012; 4:617–632. [PubMed: 22367739]

[13]. Anglicheau D, Sharma VK, Ding R, et al. MicroRNA expression profiles predictive of human renal allograft status. Proc Natl Acad Sci U S A. 2009; 106:5330–5335. [PubMed: 19289845]

[14]. Kim K, Yang DK, Kim S, Khang H. miR-142-3p is a regulator of the TGFβ-mediated vascular smooth muscle cell phenotype. J Cell Biochem. 2015; 116:2325–2333. [PubMed: 25832008]

[15]. Ulbing M, Kirsch AH, Leber B, et al. MicroRNAs 223-3p and 93-5p in patients with chronic kidney disease before and after renal transplantation. Bone. 2017; 95:115–123. [PubMed: 27866993]

[16]. Eller P, Hochegger K, Feuchtner GM, et al. Impact of ENPP1 genotype on arterial calcification in patients with end-stage renal failure. Nephrol Dial Transplant. 2008; 23:321–327. [PubMed: 17848394]

[17]. Eller P, Eller K, Kirsch AH, et al. A murine model of phosphate nephropathy. Am J Pathol. 2011; 178:1999–2006. [PubMed: 21514417]

[18]. Kirsch AH, Kirsch A, Artinger K, et al. Heterogeneous susceptibility for uraemic media calcification and concomitant inflammation within the arterial tree. Nephrol Dial Transplant. 2015; 30:1995–2005. [PubMed: 26185049]

[19]. Kirsch AH, Smaczny N, Riegelbauer V, et al. Regulatory T cells improve nephrocalcinosis but not dystrophic cardiac calcinosis in DBA/2 mice. Am J Pathol. 2013; 183:382–390. [PubMed: 23746654]

[20]. Kozina A, Opresnik S, Wong MS, et al. Oleoyl-lysophosphatidylcholine limits endothelial nitric oxide bioavailability by induction of reactive oxygen species. PLoS One. 2014; 9:e113443. [PubMed: 25419657]

[21]. Furchgott RF, Zawadzki JV. The obligatory role of endothelial cells in the relaxation of arterial smooth muscle by acetylcholine. Nature. 1980; 288:373–376. [PubMed: 6253831]

[22]. Zhang HW, Li H, Yan H, Liu BL. MicroRNA-142 promotes the expression of eNOS in human peripheral blood-derived endothelial progenitor cells in vitro. Eur Rev Med Pharmacol Sci. 2016; 20:4167–4175. [PubMed: 27775779]

[23]. Shang F, Wang SC, Hsu CY, et al. MicroRNA-92a mediates endothelial dysfunction in CKD. J Am Soc Nephrol. 2017; 28:3251–3261. [PubMed: 28696247]

[24]. Sun Y, Oravecz-Wilson K, Mathewson N, et al. Mature T cell responses are controlled by microRNA-142. J Clin Invest. 2015; 125:2825–2840. [PubMed: 26098216]

[25]. Fan HB, Liu YJ, Wang L, et al. miR-142-3p acts as an essential modulator of neutrophil development in zebrafish. Blood. 2014; 124:1320–1330. [PubMed: 24990885]

[26]. Lu X, Li X, He Q, Gao J, Liu B, Liu F. miR-142-3p regulates the formation and differentiation of hematopoietic stem cells in vertebrates. Cell Res. 2013; 23:1356–1368. [PubMed: 24165894]

[27]. Mildner A, Chapnik E, Varol D, et al. MicroRNA-142 controls thymocyte proliferation. Eur J Immunol. 2017; 47:1142–1152. [PubMed: 28471480]

Europe PMC Funders Author Manuscripts

Europe PMC Funders Author Manuscripts

Highlights

- Blood miR-142-3p is associated with pulse-wave velocity in uremic patients.
- miR-142-3p was associated with decreased vascular relaxation in uremic mice.
- Injection of miR-142-3p mimic restored acetylcholine-mediated aortic relaxation.
- miR-142-3p might prevent endothelial dysfunction and arterial stiffness in uremia.

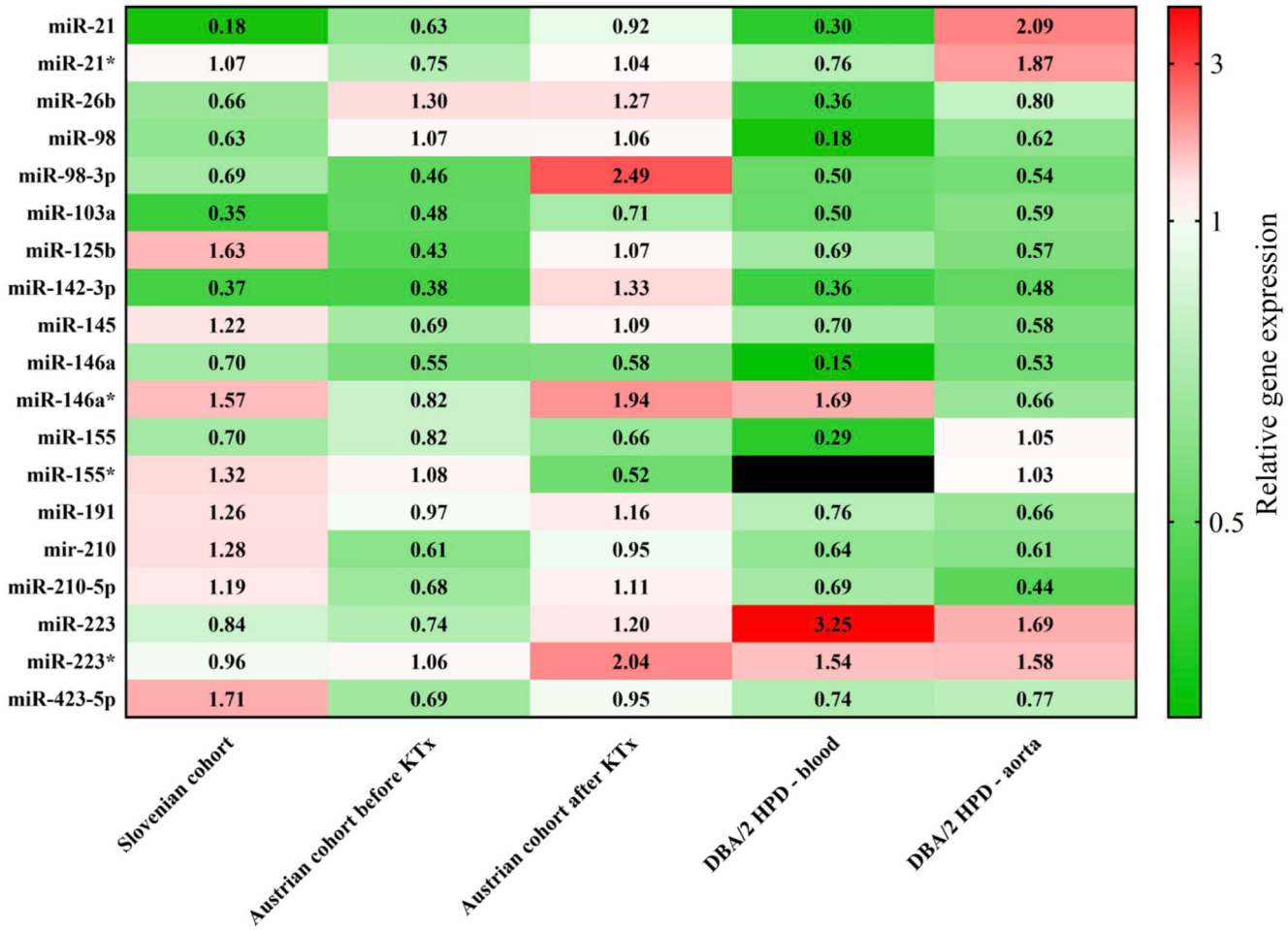

Fig. 1. Conserved miR expression patterns in mice and patients with uremia.

Expression of 19 miRs was analysed by quantitative RT-PCR in the peripheral blood of two independent CKD 5D cohorts and a subset of patients after kidney transplantation (KTx, n = 3). The data was normalized to healthy controls and the mean relative fold change is given in green for down- and in red for upregulation, respectively. Moreover, expression of the same panel was investigated in the blood and aorta of uremic DBA/2 mice and normalized to healthy controls.

Europe PMC Funders Author Manuscripts

Europe PMC Funders Author Manuscripts

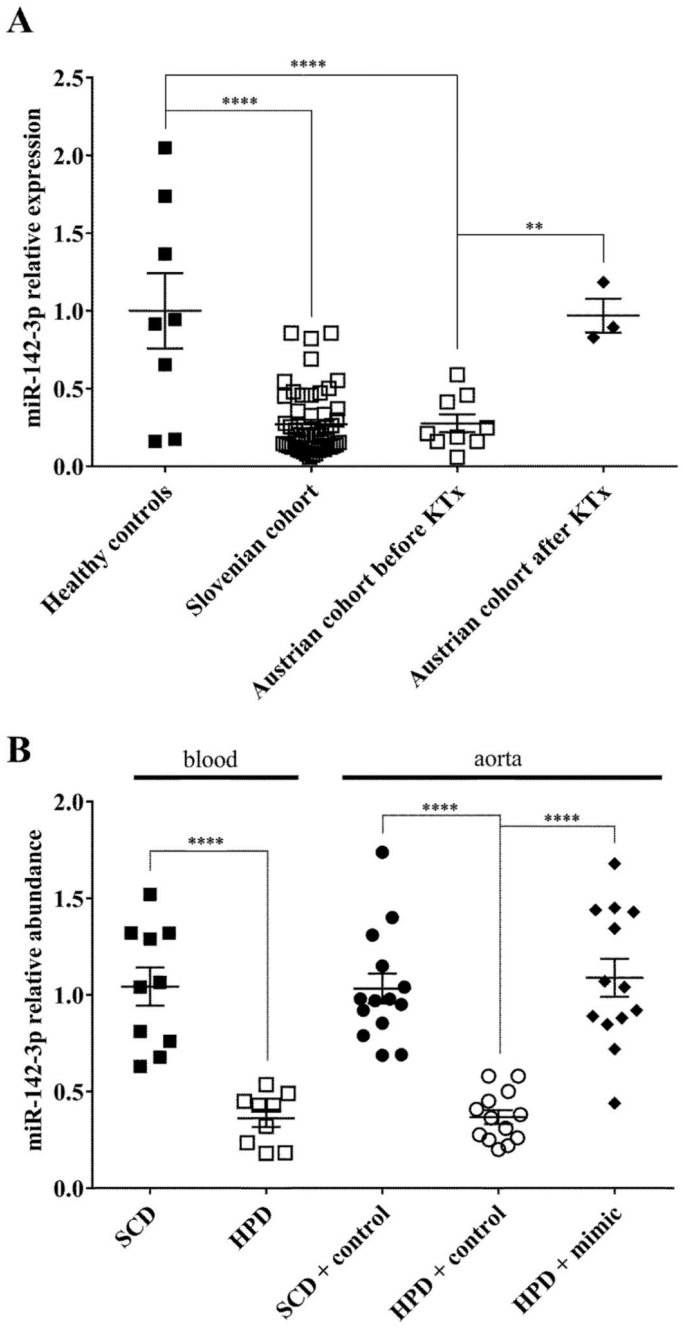

Fig. 2. miR-142-3p is downregulated in uremic patients and mice.

(A) miR-142-3p expression was analysed by quantitative RT-PCR in the blood of two independent CKD 5D cohorts (n = 53 and n = 9, open squares), and a subset of CKD patients after kidney transplantation (n = 3, closed diamonds). The expression was normalized to healthy controls (n = 8, closed squares). (B) miR-142-3p expression was analysed in the blood of DBA/2 mice on high phosphate diet (HPD) (n = 10, open squares) and compared to controls on standard chow (SCD) (n = 9, closed squares). miR-142-3p relative abundance was also measured in murine aortas with control siRNA injection (n =

13, open circles) and compared to controls on SCD (n = 14, closed circles), and mice on HPD treated with syn-mmu-miR-142-3p (n = 13, closed diamonds). Data represent mean ± SEM. * indicates $p < 0.05$; ****$p < 0.0001$.

Europe PMC Funders Author Manuscripts

Europe PMC Funders Author Manuscripts

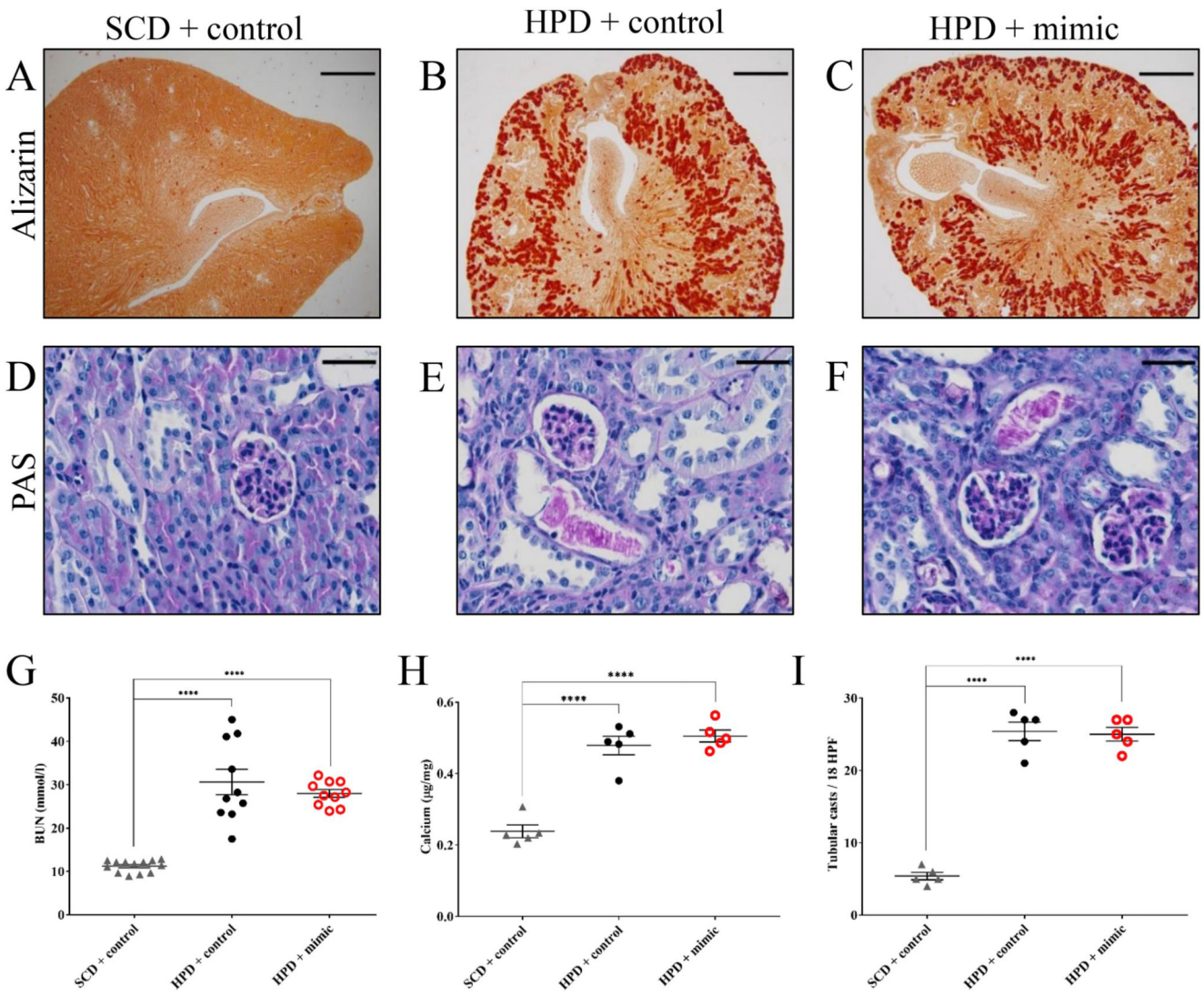

Fig. 3. Treatment with syn-mmu-miR-142-3p did not affect renal phenotype.

DBA/2 mice were fed standard chow (SCD) or high-phosphate diet (HPD), and were treated with syn-mmu-miR-142-3p mimic or negative control siRNA 48 h before the end of the experiment. The mice were divided into 3 treatment groups: SCD with control injection (A, D; grey triangles), HPD with control injection (B, E; closed circles), and HPD with mimic injection (C, F, red open circles). Renal calcification was detected by Alizarin Red S staining on kidney sections (A-C) and by measuring the total calcium content of kidneys (H). Tubular casts were counted in PAS stained kidney sections (D-F, I). Kidney function was assessed by blood urea nitrogen (BUN) levels (G). Representative images are shown (A-F). Data represent mean ± SEM. **** indicates $p < 0.0001$. The size bars display 500 μm for A-C and 25 μm for D-F.

Europe PMC Funders Author Manuscripts

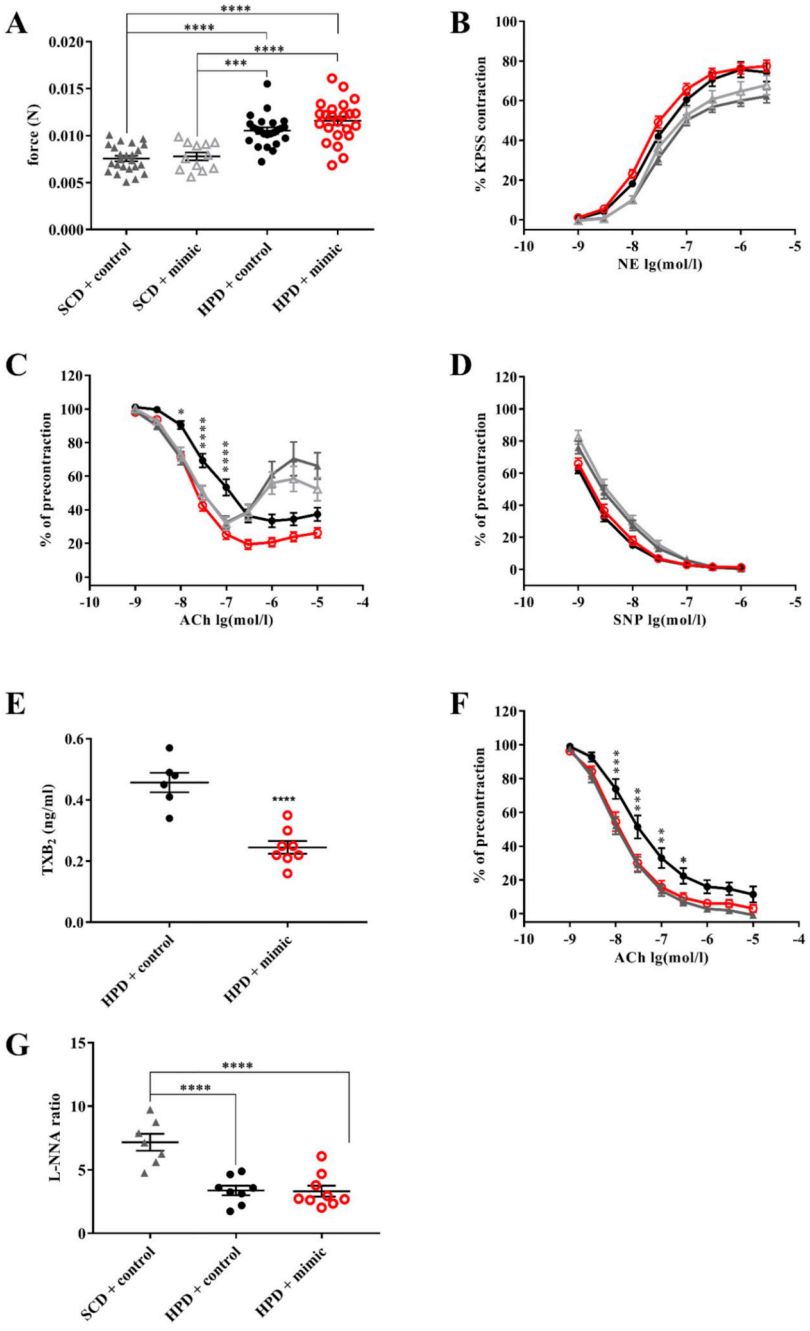

Fig. 4. Syn-mmu-mir-142-3p restores aortic relaxation attenuated by uremia.

DBA/2 mice were either fed standard chow (SCD) or high-phosphate diet (HPD) and were treated with syn-mmu-miR-142-3p mimic or negative control siRNA 48 h before the end of the experiment. Animals were divided into 4 treatment groups: SCD with control injection (grey closed triangles), SCD with mimic injection (grey open triangles), HPD with control injection (closed circles), and HPD with mimic injection (red open circles). Maximum KPSS contraction force of aortic rings (A), norepinephrine (NE)-induced contraction (B), acetylcholine (ACh)-induced relaxation of NE-precontracted aortic rings (C), and sodium

nitroprusside (SNP)-mediated relaxation of NE-precontracted aortic rings (D) were evaluated in all four treatment groups. The thromboxane B2 synthesis (TXB2) was significantly reduced in explanted aortic rings after treatment with syn-mmu-miR-142-3p mimic injection (E). The effect of syn-mmu-miR-142-3p mimic on acetylcholine (ACh)-mediated relaxation was measured after pretreatment of aortic rings with diclofenac (F). The L-nitroarginine (L-NNA)-induced endothelium-dependent constriction response in NE-preconstricted aortic rings (G) was impaired in uremic mice. Data represent mean ± SEM. * indicates $p < 0.05$, ** $p < 0.01$, *** $p < 0.001$, and **** $p < 0.0001$ between mice on HPD that were treated either by injection of syn-mmu-miR-142-3p mimic or negative control siRNA.

Europe PMC Funders Author Manuscripts

Table 1

Clinical and biochemical characteristics of patients with chronic kidney disease.

	Slovenian CKD G5D cohort	Austrian CKD G5D cohort	
	(n = 53)	Before KTx (n = 9)	After KTx (n = 3)
Gender (male; %)	68%	67%	100%
Age (years)	63.1 ± 2.0	44.9 ± 4.0	43.3 ± 7.3
Dialysis vintage (months)	61.7 ± 7.9	43.8 ± 8.4	37.0 ± 11.9
Hemodialysis	100%	0%	0%
Peritoneal dialysis	0%	100%	0%
Leukocytes (G/L)	6.0 ± 0.3	6.8 ± 0.6	7.2 ± 2.0
Hemoglobin (g/L)	112 ± 1	113 ± 6	134 ± 10
Calcium (mmol/L)	2.14 ± 0.03	2.19 ± 0.07	2.44 ± 0.04
Phosphate (mmol/L)	1.62 ± 0.05	1.62 ± 0.09	0.97 ± 0.13
Magnesium (mmol/L)	1.22 ± 0.18	1.01 ± 0.08	0.74 ± 0.04
C-reactive protein (mg/dL)	6.2 ± 0.9	2.6 ± 1.2	2.2 ± 1.4
Parathyroid hormone (ng/L)	287.1 ± 22.6	291.2 ± 48.6	142.9 ± 26.4
Creatinine (mg/dL)	9.59 ± 0.24	9.04 ± 0.99	1.67 ± 0.24
BUN (mg/dL)	134 ± 3	119 ± 9	66 ± 13
Systolic blood pressure (mmHg)	138 ± 2	132 ± 5	125 ± 3
Diastolic blood pressure (mm Hg)	75 ± 2	85 ± 4	82 ± 233%
Coumarin (%)	0%	22%	0%
Sevelamer (%)	69%	100%	0%
Cinacalcet (%)	21%	22%	0%
Calcitriol (%)	51%	44%	0%
Lanthanum carbonate (%)	6%	0%	0%
Statin (%)	31%	33%	33%
Insulin (%)	31%	0%	0%
Coronary calcium score	914 (52, 1767	139 (12, 179)	
Ca score of the ascending aorta	84 (0, 819)		
Ca score of the abdominal aorta	5655 (1356, 9990)		
Pulse wave velocity (m/s)	11.27 ± 0.43		